Materials Science & Engineering C 124 (2021) 112020

Contents lists available at ScienceDirect

Materials Science & Engineering C

journal homepage: www.elsevier.com/locate/msec

Understanding of how the properties of medical grade lactide based copolymer scaffolds influence adipose tissue regeneration: Sterilization and a systematic *in vitro* assessment

Shubham Jain [a], Mohammed Ahmad Yassin [b], Tiziana Fuoco [a], Samih Mohamed-Ahmed [b], Hallvard Vindenes [b,c], Kamal Mustafa [b], Anna Finne-Wistrand [a,*]

[a] Department of Fibre and Polymer Technology, KTH Royal Institute of Technology, Teknikringen 56-58, SE 10044 Stockholm, Sweden
[b] Tissue Engineering Group, Department of Clinical Dentistry, Faculty of Medicine, University of Bergen, Årstadveien 19, 5009 Bergen, Norway
[c] Department for Plastic, Hand and Reconstructive Surgery, National Fire Damage Center, Bergen, Norway

ARTICLE INFO

Keywords:
Degradable polymers
Adipose tissue engineering
Mechanical properties
Physical properties
Cell-material interaction

ABSTRACT

Aliphatic polyesters are the synthetic polymers most commonly used in the development of resorbable medical implants/devices. Various three-dimensional (3D) scaffolds have been fabricated from these polymers and used in adipose tissue engineering. However, their systematic evaluation altogether lacks, which makes it difficult to select a suitable degradable polymer to design 3D resorbable implants and/or devices able to effectively mimic the properties of adipose tissue. Additionally, the impact of sterilization methods on the medical devices, if any, must be taken into account. We evaluate and compare five different medical-grade resorbable polyesters with L-lactide content ranging from 50 to 100 mol% and exhibiting different physiochemical properties depending on the comonomer (D-lactide, ε-caprolactone, glycolide, and trimethylene carbonate). The salt-leaching technique was used to prepare 3D microporous scaffolds. A comprehensive assessment of physical, chemical, and mechanical properties of the scaffolds was carried out in PBS at 37 °C. The cell-material interactions and the ability of the scaffolds to promote adipogenesis of human adipose tissue-derived stem cells were assessed *in vitro*. The diverse physical and mechanical properties of the scaffolds, due to the different composition of the copolymers, influenced human adipose tissue-derived stem cells proliferation and differentiation. Scaffolds made from polymers which were above their glass transition temperature and with low degree of crystallinity showed better proliferation and adipogenic differentiation of stem cells. The effect of sterilization techniques (electron beam and ethylene oxide) on the polymer properties was also evaluated. Results showed that scaffolds sterilized with the ethylene oxide method better retained their physical and chemical properties. Overall, the presented research provides (i) a detailed understanding to select a degradable polymer that has relevant properties to augment adipose tissue regeneration and can be further used to fabricate medical devices/implants; (ii) directions to prefer a sterilization method that does not change polymer properties.

1. Introduction

Regeneration of adipose tissue aims to repair and maintain damaged tissue after trauma, injury, mastectomy, or surgical resection [1,2]. During adipose tissue regeneration in large volume defects, it is essential to help rebuild the structural integrity and function of the damaged tissue since it does not regenerate and regain the shape itself. Adipose tissue has a complex cell environment with a highly vascularized matrix [3,4] and because of this cellular heterogeneity, the regeneration of adipose tissue in a large volume defect remains a challenge. There is in fact a lack of suitable implants/grafts that can provide adequate structural and mechanical support to the cells and the newly formed tissue, while simultaneously degrade making space for extracellular matrix (ECM) [5]. In addition to increase the space for the new tissue, the degradability of an implant is an advantage in many situations since it prevents material related complications that might arise a long time after the surgery and/or repetitive surgeries to remove the implant. 3D scaffolds fabricated from degradable synthetic polymers can be a

* Corresponding author.
E-mail address: annaf@kth.se (A. Finne-Wistrand).

https://doi.org/10.1016/j.msec.2021.112020
Received 4 December 2020; Received in revised form 24 February 2021; Accepted 27 February 2021
Available online 18 March 2021

successful solution for adipose tissue regeneration thanks to the possibility to modify the structure, composition and molar mass of the polymer. This allows the mechanical properties and the degradation profile to be tuned while versatility in designing the 3D scaffolds is enabled [6–8].

Aliphatic polyesters, especially lactide (LA) based polymers are used in many FDA approved medical devices as well as in several tissue engineering applications [9,10]. For instance, poly(L-lactide) (PLLA) has been used for lipoatrophy [11], as bone implants [12], and degradable sutures [13] in clinical applications. Similarly, poly(L-lactide-*co*-glycolide) (PLGA) based scaffolds have been shown to improve adipose tissue regeneration *in vivo* and *in vitro* along with drug delivery applications [14,15]. Poly(D,L-lactide) (PDLA) and poly(ε-caprolactone) (PCL) were recently used to print 3D customized scaffolds and these showed good results in *in vivo* breast tissue regeneration [16,17]. Moreover, poly(L-lactide-*co*-trimethylene carbonate) (PLATMC) and poly(L-lactide-co-ε-caprolactone) (PCLA) have shown to be suitable for soft/adipose tissue regeneration *in vivo* and *ex vivo* [18]. A more comprehensive study was performed by fabricating six different nanofibrous scaffolds from the most common polyesters. Their mechanical properties, degradation profile and cellular response were assessed and the results demonstrated their potential use in tissue engineering applications [19]. Similarly, six different polyesters films have been compared and the results from mechanical properties and degradation *in vitro* showed their potential use in a broad range of tissue engineering applications [20]. In recent research PCL has been blended with poly(glycerol sebacate) (PGS), PLLA and PLGA to prepare nanofibrous scaffolds for the retinal degenerative disorder [21]. In the research mentioned above the polymer's physical, chemical, and mechanical properties have been mostly explored individually and their correlation with stem cells in the same system, when the aim is adipose tissue regeneration, is lacking. Therefore, selecting a polymer that can be processed into 3D scaffolds by various techniques and where the resulting 3D scaffold has physio-chemical and mechanical properties appropriate for adipose tissue regeneration remains a challenge.

The importance of the scaffold's properties and their influence in tissue engineering is evident when observing the *in vivo* microenvironment [22]. Stem cells are residing in a complex niche where a small change in the biochemical and mechanical properties tightly regulates their fate [23–25]. From a biomechanical perspective, the scaffold should have mechanical properties similar to the native niches, as stem cells are extremely sensitive toward tissue-level elasticity, which further determines their tissue-specific lineage [26]. For instance, soft matrices/scaffolds that have modulus mimicking adipose tissue enhance stem cell-derived adipogenesis while a rigid surface favors osteogenesis [27,28]. Also, the spatiotemporal properties of the 3D scaffold must provide the necessary support for cell proliferation, differentiation, and tissue vascularization. Based on the polymer processability and feasibility, the technique to create 3D scaffolds for the desired outcome can be selected [29–31]. In addition to this, scaffold design is of great importance as it alters key properties such as porosity and mechanical strength, which affect cell behavior [32].

Sterilization of the degradable 3D scaffold is another challenging task. A medical device cannot be used *in vivo* until it is free from all contamination. Hence, selecting a suitable sterilization technique is a crucial final step toward a useful scaffold or medical device. No sterilization method can be universally used for all types of polymers/scaffolds, one must be especially careful when using polymers that cannot withstand harsh conditions. In these cases, a suitable sterilization method needs to be selected in regard to the polymer and the desired application. The most common sterilization methods are ethylene oxide (ETO), radiation sterilization, such as electron beam (EB) or gamma, gas plasma, and steam/dry heat sterilization [33–35]. ETO and irradiation using EB or gamma rays are mostly utilized for scaffolds and medical devices, the methods provide sterility assurance level (SAL) of 10^{-6} [36]. Nevertheless, sterilization methods can have an impact on the polymer properties. For instance, gas plasma sterilization causes the collapse of the scaffolds' walls and pores as it requires a different pressure cycle to effectively decontaminate the porous scaffolds. ETO sterilization can be performed at low temperatures but degassing takes a longer time. In comparison, radiation sterilization can be processed at room temperature with short sterilization time and without risk of toxic residues. However, under these sterilization conditions aliphatic polyesters degrade and the degree of degradation depends on for example the polymer composition and microstructure [34,37,38].

PDLA, PLLA PLGA, PCLA and PLATMC have been used in several tissue engineering applications but the quest for the polymer that has the most suited physio-chemical and mechanical properties for adipose tissue regeneration remains elusive due to the lack of a comprehensive study which includes all polymers. Therefore, in this research, these five commercially available degradable synthetic polymers of medical-grade with different physiochemical properties have been systematically compared and assessed for their potential in adipose tissue regeneration.

Our objective was to systematically characterize cell-material interactions and understand how physio-chemical and mechanical properties of the above-named polymers influence stem cell behavior. We also aimed to determine an optimal sterilization method that is easy, efficient, and does not alter critical polymer or scaffold properties. To fulfill the aim, we prepared 3D scaffolds using salt-leaching method and the polymer properties were characterized in detail. Additionally, *in vitro* evaluation was performed using human adipose tissue-derived stem cells (ASC) and assessed cellular events in terms of cell attachment, proliferation, and differentiation toward adipose tissue regeneration. Furthermore, scaffolds were sterilized using EB and ETO, their physical, chemical, and mechanical properties were characterized before and after sterilization. Fig. 1 summarizes the overall approaches used in the presented research.

2. Material and methods

2.1. Preparation of scaffolds using the salt leaching technique

Porous scaffolds were prepared using the salt particulate leaching technique as described earlier [39].]. Briefly, a 10% *w/v* solution was prepared by dissolving each polymer in chloroform and the solution was poured into glass Petri dishes containing NaCl particles of 75–500 μm sizes (polymer to salt ratio of 1:10). The solution was mixed with salt particles homogeneously and left for slow drying. Later, the dried polymer film was taken out of the Petri dishes and scaffolds punched out in a cylinder shape (11 mm in diameter and 1 mm in height). Scaffolds were then leached out in deionized water and vacuum dried prior to use.

2.2. Characterization of the scaffolds

2.2.1. Scanning electron microscopy (SEM)

SEM (JSM 7400F, JEOL, Japan) was used to analyze the surface morphology of the scaffolds. A platinum/palladium coating (~10 nm) was used to sputter the scaffolds before imaging at 5 kV.

2.2.2. Micro-computed tomography (micro-CT)

A micro-CT imaging system (SkyScan 1172, Bruker, Kontich, Belgium) was used to characterize 3D scaffolds and calculated volume (mm^3), surface area (mm^2), and porosity (vol%). Each scaffold was scanned at 40 kV, 250 mA, and no filter. NRecon and CTan software (SkyScan, Kontich, Belgium) were used for volumetric reconstruction and image analysis. A cylindrical volume of interest (VOI) with 10 mm in diameter and 1 mm in height was selected ($n = 3$ per each group).

2.2.3. Differential scanning calorimetry (DSC)

Thermal properties: glass transition temperature (T_g), melting point (T_m), and degree of crystallinity were measured using a Mettler Toledo DSC 1 instrument. An aluminum pan was used to record the DSC

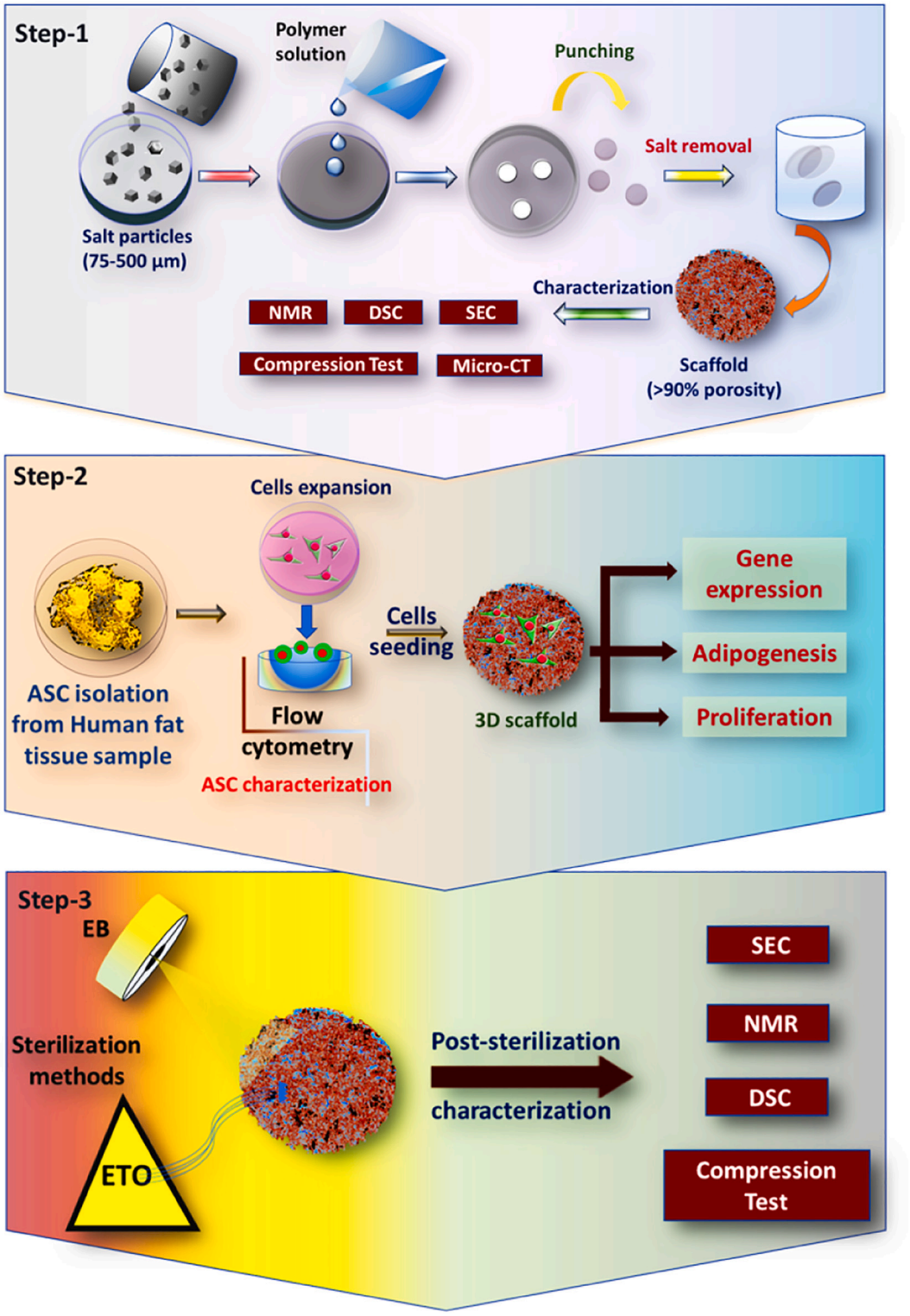

Fig. 1. Schematic overview of the research approaches used. Step 1: Preparation of the 3D scaffolds using salt-leaching technique and subsequent characterization of the polymer's physio-chemical and mechanical properties. Step 2: Stem cell isolation, characterization using flow cytometry and evaluation of their interaction with 3D scaffolds for adipogenesis. Step 3: Comparing the polymer properties before and after sterilization by EB and ETO.

thermogram and the instrument was calibrated using indium. A heating ramp of 10 °C min^{-1} was used to heat the sample under an inert atmosphere and a thermogram recorded from −20 to 220 °C. T_g and T_m were obtained from the first heating run. The reported values for T_g are from Midpoint ASTM, calculated using Mettler Toledo STARe v. 15.00 software. Enthalpy of fusion for pure PLA crystal (ΔH_m^o) of 93.0 Jg^{-1} [40] was used to calculate the percentage degree of crystallinity (X_c) using the following equation:

$$X_c = [(\Delta H_m - \Delta H_c)/\Delta H_m^\circ] \times 100$$

2.2.4. Size exclusion chromatography (SEC)

Number-average molar mass, mass-average molar mass (M_n and

M_w), and the dispersity (Đ) were determined using SEC. The measurements were taken at 35 °C temperature utilizing a Verotech PL-GPC 50 Plus equipped with a PL-RI detector and two columns (PLgel 5 μm MIXED-D). Chloroform was used as an eluent phase and a calibration curve was prepared using polystyrene standards with low dispersity. Internal variations were corrected using toluene as internal standard.

2.2.5. Nuclear magnetic resonance (NMR)

Deuterated chloroform ($CDCl_3$) was used to dissolve the scaffolds and proton (^1H) and carbon (^{13}C) NMR spectra were recorded using Bruker top spin software on Bruker 400 Ultrashield spectrophotometer. MestReNova software was used to analyze the spectra.

2.2.6. Contact angle and water uptake

The water contact angle was measured on solvent casting films by placing a MilLi-Q water drop of 3 μl and the angle was calculated using CAM 200 software. Measurements were taken at room temperature. The data presented here are the mean from three different samples.

Scaffolds were initially weighed and soaked in PBS, kept at 37 °C. After 24 h, scaffolds were taken out and excess water was wiped off using a paper towel and weighed, water uptake was calculated as follows: Water uptake (%) = $(M_t - M_0) / M_0 \times 100$; where M_t is the weight at time t and M_0 is the weight of dry scaffolds.

2.2.7. Compression test

The compression tests were conducted using two different conditions: room temperature (in a dry state; 23 °C with 50% humidity) and at 37 °C, in wet condition. Scaffolds were preincubated in PBS for 5 min and then tested. The specimens (cylindrical shape) were cut in an approximate dimension of 4.5 mm in thickness and 5.5 mm in diameter. A custom-made setup was built to test the specimens in a wet condition which was attached to the Universal tester Instron 5566 (Instron Corporation, High Wycombe, UK) at both conditions. Scaffolds after electron beam sterilization were tested using a regular Instron setup. A 100 N load and a compression rate of 10% thickness/min were employed to take measurements, recorded using Bluehill software. The Young's modulus was calculated as slope of the tangent of initial linear region (between 0 and 20% of strain) of the stress-strain curve.

2.3. Cell-material interactions

2.3.1. Adipose stem cell (ASC) isolation, expansion, and characterization

ASC were isolated from human fat tissue samples obtained from patients who underwent routine surgery at Haukeland University Hospital, Bergen, Norway, with proper consent, under ethical approval from the REK (Regional committees for medical and Health Research Ethics 2013/1248/REK).

ASC were isolated as described previously [41]. Briefly, the adipose tissue block was washed with an antibiotic solution (5% in PBS), minced, and digested by 0.1% collagenase type 1 solution containing 2% antibiotic in PBS, for 1 h at 37 °C. After an hour, an equal amount of growth culture medium [Dulbecco's Modified Eagle Medium (DMEM) with 10% fetal bovine serum and 1% penicillin-streptomycin] was added to neutralize the collagenase activity and cells were centrifuged at 2000 rpm for 5 min. The pellet was shaken, recentrifuged and supernatant fluid was suctioned off. The pellet was then resuspended in growth medium (GM) and plated in T75-tissue culture flask for cell growth in a humidified incubator at 37 °C with 5% CO_2. ASC were expanded and cells at passages 3–5 were used for the *in vitro* assessment. Cell morphology was monitored during the culture.

Prior to using ASC in the experiments, cells were characterized using flow cytometry, based on specific cell surface antigens, as reported previously [41]. The cells were incubated with the fluorescent antibodies of the specific cell surface antigens, following the manufacture's protocols. Multi-lineage differentiation capacity of the cells was examined based on differentiation into osteogenic, adipogenic and chondrogenic lineages.

2.3.2. Cell seeding, attachment, and proliferation

Scaffolds were sterilized using 70% ethanol and Ultraviolet light-C (UV), then washed three times with PBS. Samples were placed in a 48 well plate and entrapped air removed by centrifugation through adding GM. Scaffolds were then soaked in GM overnight. A cell suspension of 100 μl (1.5×10^5 cells) was added on each scaffold, the scaffolds were submerged with adequate GM, and cells were to attach for an hour. Next, additional GM was added and refreshed every three days during the experiment. For SEM, seeded cells were fixed following a previously used protocol [24].

Cell proliferation was assessed on days 7 and 14 using Picogreen assay (Thermo Seientific, USA) as described previously [42]. In short, the culture medium was aspirated, and the samples were washed with PBS. A 0.25 ml of lysis solution (0.02% sodium dodecyl sulfate and 0.2 mg^{-1}) was added to each well containing a scaffold and kept at 37 °C for 12 h. The lysate was collected in 96 well plates and an equal amount of Picogreen dye was added. The fluorescence was recorded at 485 nm excitation and 520 nm emission wavelengths in microplate reader (Thermo Scientific, USA). Furthermore, confocal microscopy (Leica SP8, Leica microsystems and Andor Dragonfly 505 confocal) was used to evaluate cell morphology and distribution on 3D scaffolds by following a previously used protocol [43].

2.3.3. Adipogenic differentiation

Adipogenic differentiation was assessed by culturing ASC in an adipogenic medium (AM) for 21 days. AM was prepared by adding the adipogenic supplements 3-isobutyl-1-methylxanthine (IBMX) (500 μM), dexamethasone (1 μM), insulin (10 μg/ml and indomethacin (100 μM) to the GM. AM was added after 3 days of cell seeding and counted day 1.

Oil Red O (ORO) dye was used to stain the neutral lipid droplets on the scaffolds after 21 days in AM. Briefly, 4% paraformaldehyde was used to fix the cells at room temperature for 30 min and subsequently washed with PBS. Later, samples were incubated with 60% isopropanol for 5 min, and then 0.3% of ORO solution was added to each well-containing scaffold, for 25–30 min. The scaffolds were then washed repeatedly with distilled H_2O until no dye came out with water. The bound dye was extracted using 100% isopropanol and absorbance was recorded at 540 nm using a spectrophotometer (BMG LABTECH, GmbH, Germany). Digital photographs were taken before extracting the dye for visual proof.

Intracellular lipid droplets were visualized fluorescently by the AdipoRed™ assay (Lonza Walkersville, Inc., USA) following the supplier's protocol. Briefly, scaffolds were fixed, washed with PBS, and incubated with 12 μl of dye in 400 μl of PBS for 10 min. Later, scaffolds were imaged using a confocal laser microscope (Leica SP8, Leica microsystems).

2.3.4. Real Time Quantitative Polymerase Chain Reaction (real-time qPCR)

Expression of selected adipogenic genes was assessed by culturing ASC on scaffolds in AM for 21 days to further confirm the adipogenic differentiation. Maxwell® RNA extraction kit (Promega, USA) was used to isolate total RNA from the cells, following the manufacture's protocol. The quality and amount of RNA were determined using the nanodrop spectrophotometer (Nanodrop Technologies, USA). cDNA synthesis was performed using a High-Capacity cDNA Reverse Transcriptase kit (Applied Biosystem, USA) from 300 ng of RNA. Real-time qPCR was performed using TaqMan Fast Universal PCR master mix and the StepOne™ real-time PCR system (Applied Biosystem). We selected, PPARG (peroxisome proliferator-activated receptor gamma), CEBPA (CCAAT enhancer binding protein alpha), LPL (lipoprotein lipase), and ADIPOQ (adiponectin, C1Q and collagen domain containing genes) genes and assessed adipogenic differentiation. GAPDH (Glyceraldehyde-3-phosphate dehydrogenase) was used as an internal control. Table 1 lists the

Table 1
Primer sequence used for gene expression analysis.

Gene	Amplicon length	Gene ID
GAPDH	93	Hs02758991_g1
PPARG	77	Hs00234592_m1
CEBPA	77	Hs00269972_s1
LPL	103	Hs00173425_m1
ADIPOQ	71	Hs00605917_m1

details of the adipogenic genes and primer sequences used.

2.4. Post-sterilization characterization

The most widely used sterilization methods for medical devices are ETO and EB. Herein, both methods were used for sterilization, and scaffolds were characterized afterward to see if methods have any effect on the polymer properties.

ETO sterilization was performed using ANDERSEN sterilizers, United Kingdom, at room temperature in an AN4000.11 series 4 cabinet (procedure number: AQD 225 V.11). The duration of the ETO gas cycle was 12 h and degassing was performed for 48 h at RT. EB sterilization was done according to the ISO 1137 standard for health care products. Briefly, samples were packed in an inert atmosphere and a dose of 25 kGy was used by using a 6.5 MeV pulsed electron-beam accelerator (Mikotron, Acceleratorteknik, Stockholm, Sweden). The samples were placed on a cooling plate during radiation. Methods used were able to achieve a sterility assurance level of 10^{-6}.

2.5. Statistical analysis

Quantitative data were obtained from at least four replicates and presented as mean ± SD. Origin 8.0 software was used to calculate significant differences, performing ANOVA one-way analysis with Tukey's test. Significant differences ($P < 0.05$) were denoted as symbol *.

3. Results and discussion

3.1. Characterization of the scaffolds

There are several different methods available for preparing microporous 3D scaffolds to mimic tissue-like architecture that supports cell growth for tissue engineering applications. Due to the simple fabrication process, particulate leaching methods are the most widely used among the different available methods such as freeze-drying and solvent casting [39,44]. We selected 5 different medical grade degradable polymer and copolymers that are available commercially: PLLA, PDLA, PCLA, PLGA, and PLATMC with L-lactide content ranging from 50 to 100 mol% to prepare microporous scaffolds.

SEM and Micro-CT results revealed that scaffolds had interconnected pores and porous architecture (Fig. 2), which is a prerequisite for functional tissue engineering 3D construct, allowing cellular infiltration and migration into the pores, and mimicking tissue-like microenvironment. We determined the pore size distribution and porosity using Micro-CT, which showed that all scaffolds independent of polymer had similar pore size/volume distribution (Fig. 3a) with ≈92% porosity and showing structural similarity in pore size of the 3D scaffolds.

The thermal properties of the scaffolds were determined using DSC. Results, summarized in Table 2, revealed that PLLA, PCLA, and PLGA were semi-crystalline and showed 51, 20, and 3.5% X_c, respectively. PDLA and PLATMC were amorphous. T_g is another factor that influences scaffolds' pliability and softness and when scaffolds are intended to use for adipose or soft tissue, they must be soft. PLLA, PDLA, and PLGA scaffolds showed T_g of 60, 59, and 60 °C, correspondingly. In contrast, PCLA and PLATMC showed a similar T_g of 28 °C which is lower than the body temperature (37 °C). The lower T_g is probably an advantage for adipose/soft tissue application as scaffolds become softer at physiological conditions, which can further prevent possible tissue damage due to sharp edges.

Surface hydrophilicity of the scaffolds is one important property that can influence the focal adhesion proteins which further modulate stem cell fate [45]. The wettability of the polymer is largely influenced by the comonomer units' and functional groups' arrangement in a polymeric chain. We prepared solvent cast polymer films to evaluate the surface hydrophilicity of the polymers by measuring the water contact angle. Results showed that PCLA and PLATMC had the highest average contact angle values of 84 ± 3 and 83 ± 3°, respectively, among all the polymers (Fig. 3 (b)). This can be attributed to the presence of the caprolactone units in the PCLA, and trimethylene units in PLATMC which makes it more hydrophobic. PLGA had a lower contact angle values (77 ± 2) than the PLATMC and PCLA; indeed, glycolide units are considered to be more hydrophilic than the lactide units. Similarly, PLLA and PDLA had a contact angle of 79 ± 2 and 78 ± 2, respectively. However, this difference in contact angle values (77 ± 2 to 84 ± 3) might not be sufficient in influencing cell behavior especially in a 3D porous scaffold.

Furthermore, we checked the water uptake capacity of the 3D scaffolds after 24 h. Fig. (3c) summarizes the results, revealing that PLGA had the highest water uptake among all the polymers due to the presence of the glycolide units. Interestingly, we did not find any significant difference between PLLA, PDLA, PCLA, and PLATMC scaffolds. Water uptake of the polymeric scaffolds not only depends on the surface hydrophilicity but is also influenced by the polymer crystallinity and T_g. This was seen in PLATMC and PCLA scaffolds. Although the contact angle was higher than PLLA and PDLA, the water uptake in PLATMC and PCLA scaffolds was similar. This might be because PLATMC and PCLA scaffolds were above their T_g at 37 °C, which led to higher chain mobility hence more water penetration. Based on the results here, it can be concluded that water uptake by the scaffold is largely affected by both the T_g and X_c, in a synergistic manner, since there is not much difference in surface hydrophilicity of the polymers.

Scaffold design, porosity, and polymer composition largely affect the mechanical properties of the scaffolds. Typically, stiff materials show high moduli compared to soft matrices and that affects the cell-material interactions further [46,47]. Researchers usually evaluate mechanical properties of the scaffolds/implant in a dry state at RT but the fact that under physiological conditions in the body mechanical properties change due to the presence of the body fluids cannot be disregarded. Therefore, here we have evaluated the mechanical properties of the scaffolds at 37 °C in PBS (pH 7.4) by stimulating the body conditions and compared them to the ones at RT in a dry state. Fig. 3 (d) and (e) represents the compressive stress-strain curve at 37 °C and RT, respectively.

The test results at RT (Fig. (3f)) revealed that PLLA had higher elastic modulus than the others. Indeed, PLLA had the highest degree of crystallinity (X_c = 51%) among all the polymers, and M_n also was significantly higher than PDLA, PCLA, and PLATMC. PDLA and PLGA had higher modulus than PCLA and PLATMC, where the M_n of PLGA was the highest among all polymers, and PLGA had X_c of 3.5%. The results can be explained by the fact that mechanical properties are known to be affected by M_n, X_c and T_g. PCLA and PLATMC showed similar modulus and were the lowest among all. This could be because these polymers had the lowest M_n and has a T_g around RT in contrast to PLLA, PDLA, and PLGA that all have a T_g well above the room temperature (Table 2). When polymers are at a temperature above their T_g they are in the rubbery state and have more chain mobility, becoming softer as their modulus decreases. In addition, owing to the presence of CL and TMC units in the lactide chain in PCLA and PLATMC, respectively, causes the plasticization effect which further facilitate chain movement easier and exhibiting a good elastic response [48,49]. Based on our results, PCLA and PLATMC scaffolds are softer than the other scaffolds.

The tests at 37 °C revealed that, overall, all scaffolds had a significant decrease (minimum 40% for all scaffolds) in modulus compared to that

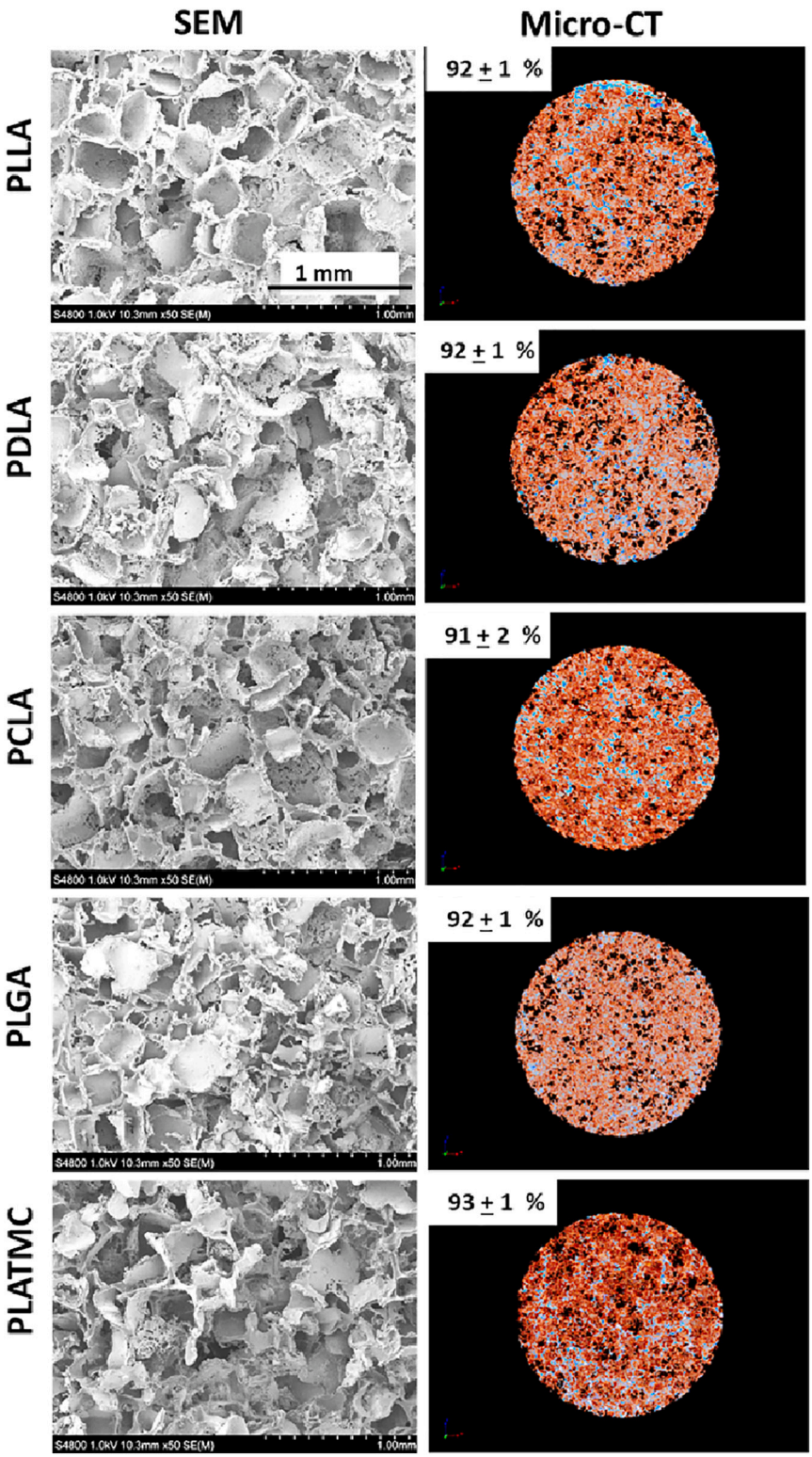

Fig. 2. Scaffolds morphology, internal architecture including porosity visualized by the SEM and Micro-CT.

of RT. Indeed, scaffolds had almost 92% porosity which makes it easy for water molecules to diffuse into the scaffold interior making scaffolds swollen and facilitating movement of the macromolecule chain segments. The result showed that PLATMC had a massive decrease (>90%) in moduli and showed the lowest (≈ 1 kPa) compressive moduli among all, and PLLA had the highest (≈365 kPa), although it decreased by 42% than RT. Similarly, PDLA, PCLA, and PLGA had a decrease of 77, 70, and 40% in their moduli compared to that of RT. PCLA had the second-lowest moduli preceded by the PDLA, PLGA which were approximately 107, 42, and 166 kPa, respectively. Interestingly, the highest water uptake was shown by the PLGA scaffolds but the decrease in moduli was less than PDLA, PCLA, and PLATMC. This can be reasoned to the higher M_n and higher T_g along with some order of crystallinity, for PLGA scaffolds. Whilst, in the PLATMC scaffold, they were above their

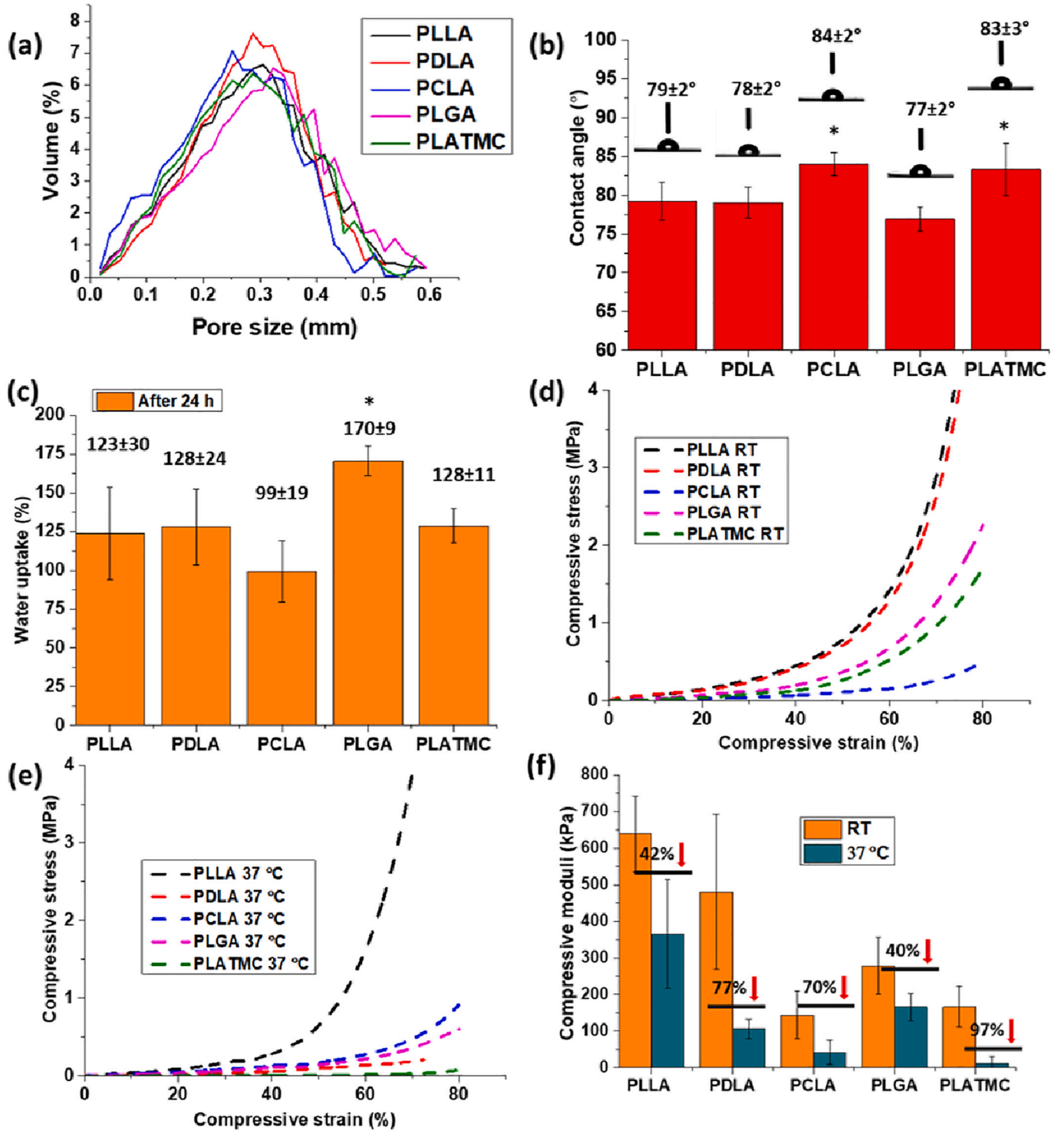

Fig. 3. Scaffold characterization: (a) Pore size distribution calculated from the Micro-CT (b) Water contact angle of the polymer films, mean ± SD. *$P < 0.05$ represents significant difference compared to PLGA. (c) Water uptake of the scaffolds after 24 h at 37 °C, represented as mean ± SD, *$P < 0.05$. (d) Compressive stress-strain curve of scaffolds at room temperature (RT) in dry condition (e) Stress-strain curve of scaffolds at 37 °C in wet condition (f) Computed compressive moduli of the scaffolds in different conditions: RT and 37 °C, and showing percentage decrease in moduli from RT to 37 °C.

T_g making polymer chain even more flexible, becomes softer. In addition, close packing of polymer chains, such as crystalline polymers, where chain motions are limited rendering them stiffer, exerts a high modulus. This can be seen here for PCLA scaffolds, even though above their T_g, the modulus of the scaffolds was higher than PLATMC, although it was lower when specimens tested at RT in a dry state. This can be attributed to the semi-crystalline ($X_c = 20\%$) nature of the PCLA scaffolds. Similar behavior was observed between highly crystalline PLLA and amorphous PDLA. It was therefore concluded that amorphous polymer having a low T_g can be advantageous in designing soft scaffold/implants for adipose tissue.

Table 2
Characterization of the scaffolds.

Polymer	M_n (kg mol^{-1})[a]	Đ[a]	L-lactide (mol%)[b]	L_{LL}[c]	L_x[c]	T_g (°C)[d]	T_m (°C)[d]	X_c (%)[e]
PLLA	196 ± 10	1.3	100	–	–	61	180	51
PDLA	178 ± 6	1.4	50	–	–	59	–	–
PCLA	138 ± 1	1.5	70	5.8	2.2	27	160	20
PLGA	249 ± 6	1.3	83	5.8	1.3	60	153	3.5
PLATMC	154 ± 3	1.4	60	2.3	1.5	28	N·O.	N.O.

[a] Number average molar mass and dispersity determined by SEC using calibration curve from polystyrene standard with low dispersity in $CHCl_3$.
[b] Obtained from ^1H NMR spectra in $CDCl_3$.
[c] Determined by ^{13}C NMR spectra where L_{LL} is the lactide block length and L_x signifies the block length of the particular comonomer used.
[d] T_g, T_m, and X_c data were obtained from the first heating run of DSC.
[e] The crystallinity, X_c, (%) was calculated from the first heating run, N.O = not observed.

3.2. Biological studies

3.2.1. Phenotypic characterization of the stem cells

Mesenchymal stem cells (MSC) are widely used in adipose tissue regeneration [50,51]. These cells are characterized by plastic adherence, negative and positive expression of cell-specific CD markers, in addition to differentiation potential toward adipogenic osteogenic and chondrogenic lineages ASC were successfully isolated from the adipose tissue samples and became adherent to the plastic tissue culture flask, showing fibroblastic morphology (Fig. 4a). ASC were positive for the stem cell markers CD73, CD90, and CD105. In addition, CD34, CD45, and HLA-DR were negative (Fig. 4b), which agreed with previous reports [52]. Fig. 4(c) shows ASC ability to differentiate into multiple lineages: adipogenic osteogenic, and chondrogenic, which is confirmed by Oil Red O, Alizarin Red, and Alcian blue staining, respectively.

3.2.2. Cell-material interactions

In general, a variety of cells from the different tissues respond not only to biochemical signals but also to mechanical cues that further regulate cell fate. MSC sense the substrate stiffness and respond by controlling the cell structure, rearranging internal cytoskeleton stress, and stiffness through a mechanism known as mechano-transduction [53–55]. Moreover, scaffold mechanical properties control the stem cell fate and stimulate the proliferation and differentiation accordingly. Hence, it is crucial that the scaffold matches the mechanical properties of the intended tissue and that it provides an internal micromechanical environment that promotes extracellular matrix organization and *de novo* synthesis [56,57]. Adipose tissue has mechanical properties in the range of 2–25 kPa which suggests that a scaffold with an elastic modulus in this range would be suitable for adipose tissue regeneration [58].

Since scaffolds have varied physiochemical and mechanical properties, we further examined ASC proliferation response on the different porous scaffolds, by measuring the DNA content using Picogreen dye. Fig. 5 shows the total DNA content of ASC cultured on the scaffolds at days 7 and 14 after cell-seeding.

On day 7, measured DNA content was higher in cells cultured on PCLA and PLATMC scaffolds compared to other scaffolds. There was no significant difference observed between PCLA and PLATMC, and between PLLA, PDLA, and PLGA scaffolds. The higher cell proliferation in PCLA and PLATMC scaffolds can be attributed to their lower modulus compare to other scaffolds which is in close range to the mechanical

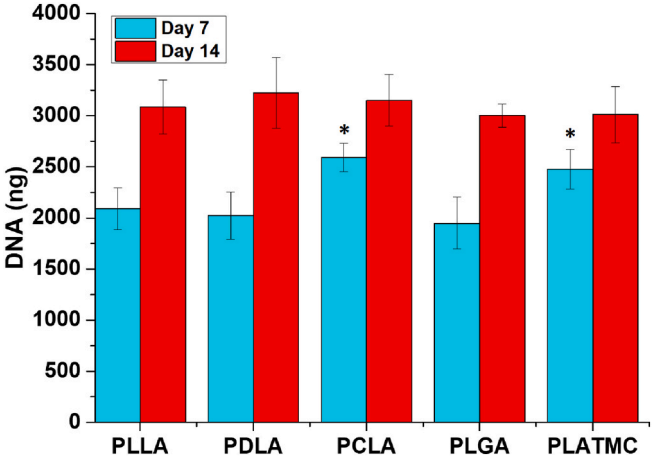

Fig. 5. DNA quantification of ASC cultured on the 3D scaffolds at day 7 and day 14 in GM. Significant differences are represented by * $P < 0.05$.

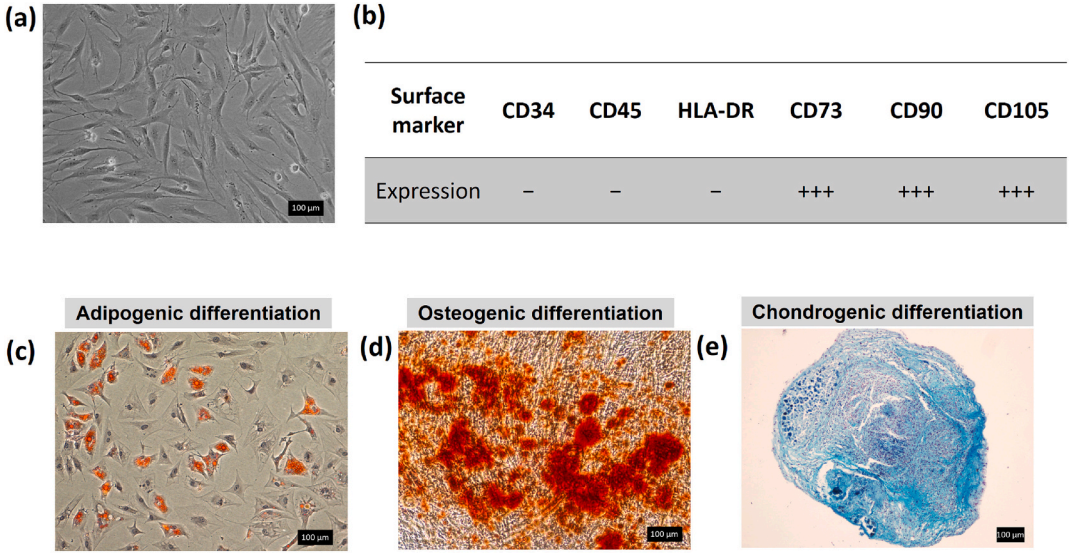

Fig. 4. ASC phenotypic characterization (a) Plastic adherent ASC under microscope (b) Immunophenotypic characterization based on surface marker expression using flow cytometry (c) Differentiation of ASC toward adipogenic, osteogenic and chondrogenic lineages, confirmed by positive staining to Oil Red O (ORO), Alizarin Red, and Alcian blue stains, respectively. (For interpretation of the references to color in this figure legend, the reader is referred to the web version of this article.)

property of the adipose tissue (2–25 kPa). Also, only these scaffolds were above their T_g at 37 °C, making polymer chains more flexible with better transport properties. Previously a study demonstrated that polycaprolactone (PCL) foam showed a higher proliferation of urinary bladder stromal cells than PLGA due to the closer match of the modulus to that of the native tissue [81]. SEM and confocal micrograph corroborated these observations (Fig. 6). Moreover, on day 7, it was observed that cells covered almost the entire area in PCLA and PLATMC. On day 14, DNA content had increased from day 7 in all scaffolds and no significant differences were observed among all the scaffolds.

3.2.3. Gene expression and adipogenic differentiation

We further evaluated the potential of the 3D porous scaffolds for adipogenic differentiation by studying the gene expression of the selected adipogenic genes PPARG, CEBPA, LPL, and ADIPOQ on day 21 by culturing ASC on scaffolds in the presence of the adipogenic supplements. Since all scaffolds are based upon lactide-based copolymers we decided to use PLLA as a control to compare the gene expressions. Fig. 7 shows the relative mRNA expression of the adipogenic genes normalized to PLLA, GAPDH expression was used as an internal control.

PPARG and CEBPA are the key regulators in the adipogenic differentiation process of becoming mature adipocytes from pre-adipocytes,

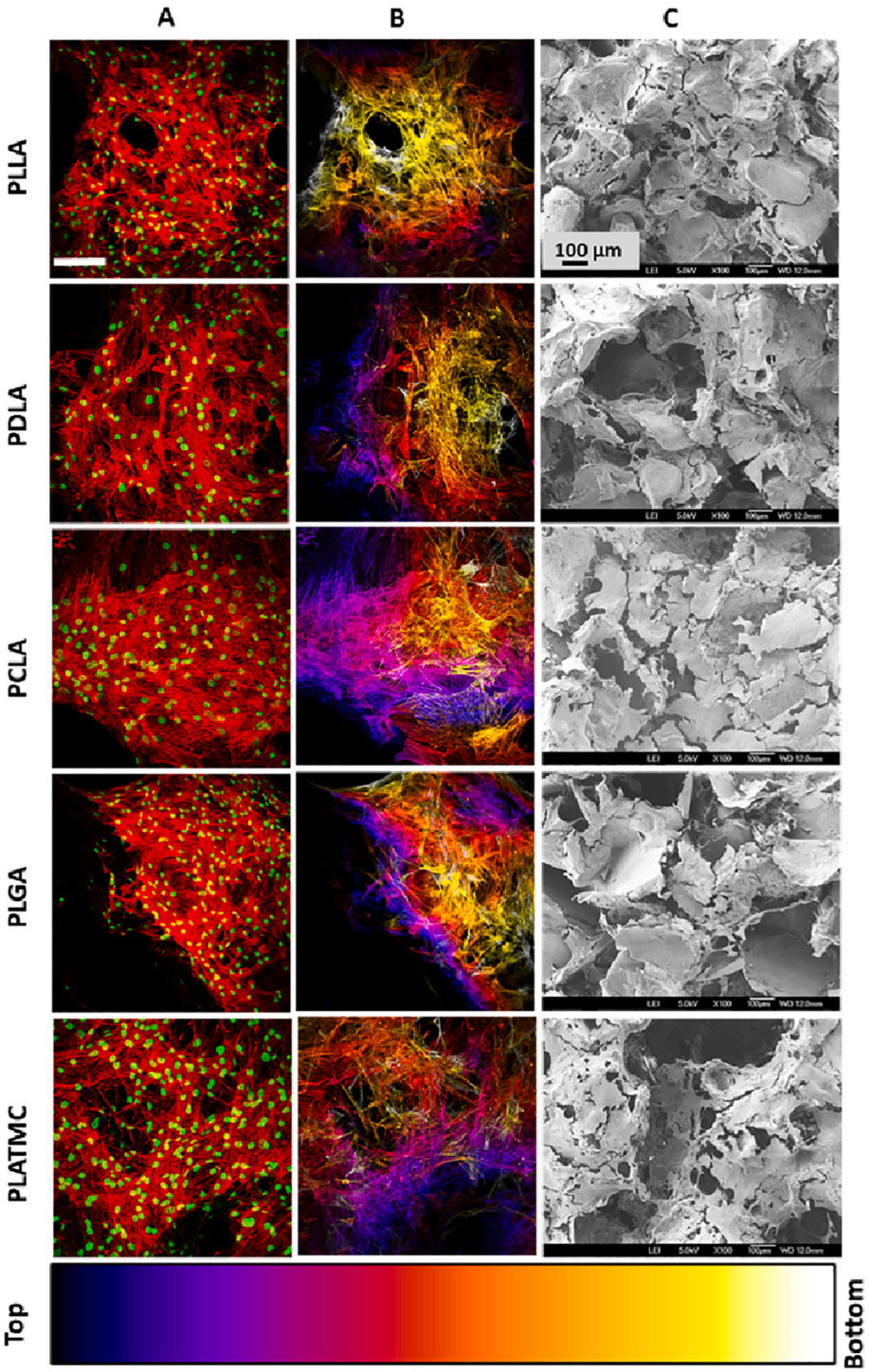

Fig. 6. ASC response on the 3D scaffolds (a) Confocal micrograph (day 7) showing cell distribution and proliferation on the scaffolds; Actin (red), nucleus (green), scale bar 100 µm. For better contrast false color were given using ImageJ (b) A depth color code representation of the ASC showing distribution inside the scaffolds. (c) SEM images of the ASC cultured on the 3D scaffolds (day 7). (For interpretation of the references to color in this figure legend, the reader is referred to the web version of this article.)

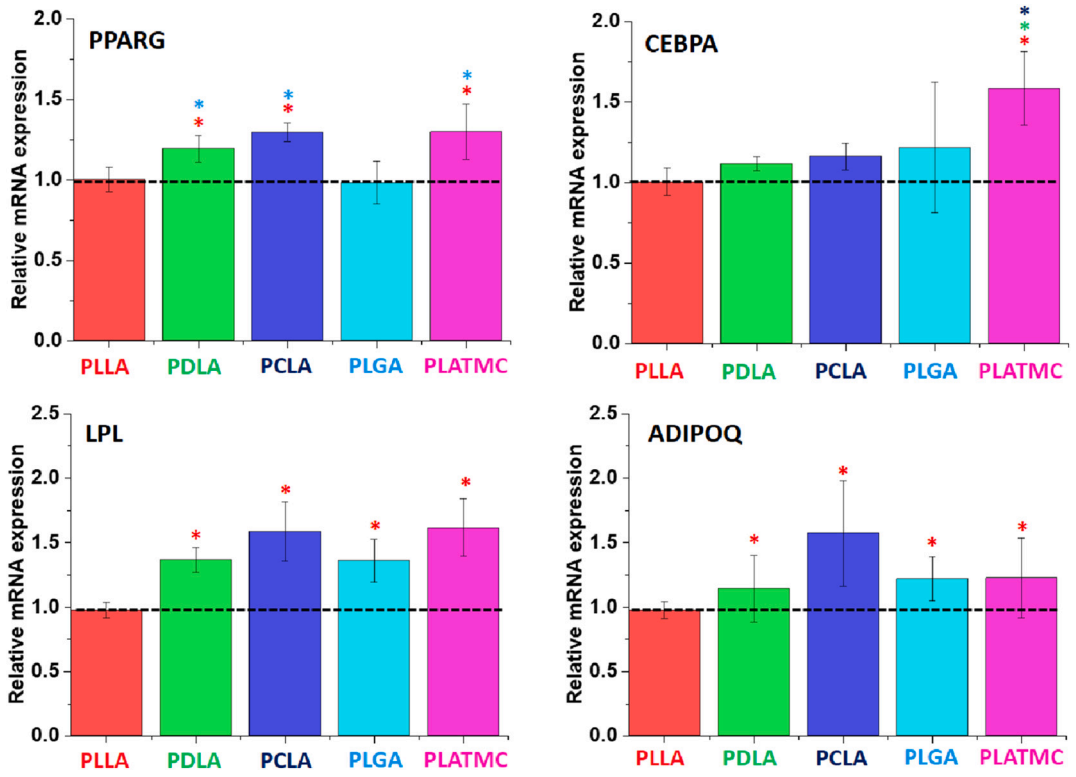

Fig. 7. Relative mRNA expression of the ASC cultured on 3D scaffolds after 21 days in AM. The presented data are normalized to PLLA and GAPDH was used as an internal control. Significant differences ($P < 0.05$) from PLLA, PDLA, PCLA, PLGA and PLATMC are indicated by color symbols *, *, *, * and *, respectively.

and PPARG is a master regulator [59]. On day 21, we found a significantly higher expression of the PPARG in PCLA, PLATMC, and PDLA scaffolds compared to PLGA and PLLA. In contrast, PLGA and PLLA showed no significant difference among them. PPARG expression makes a cooperative loop with CEBPA and promotes the expression of CEBPA and other adipogenic genes. CEBPA expression was only significantly higher on PLATMC scaffolds.

We further assessed the expression of the LPL which is secreted by the mature adipocyte and considered as an early marker of the adipogenic differentiation. LPL expression increases throughout the

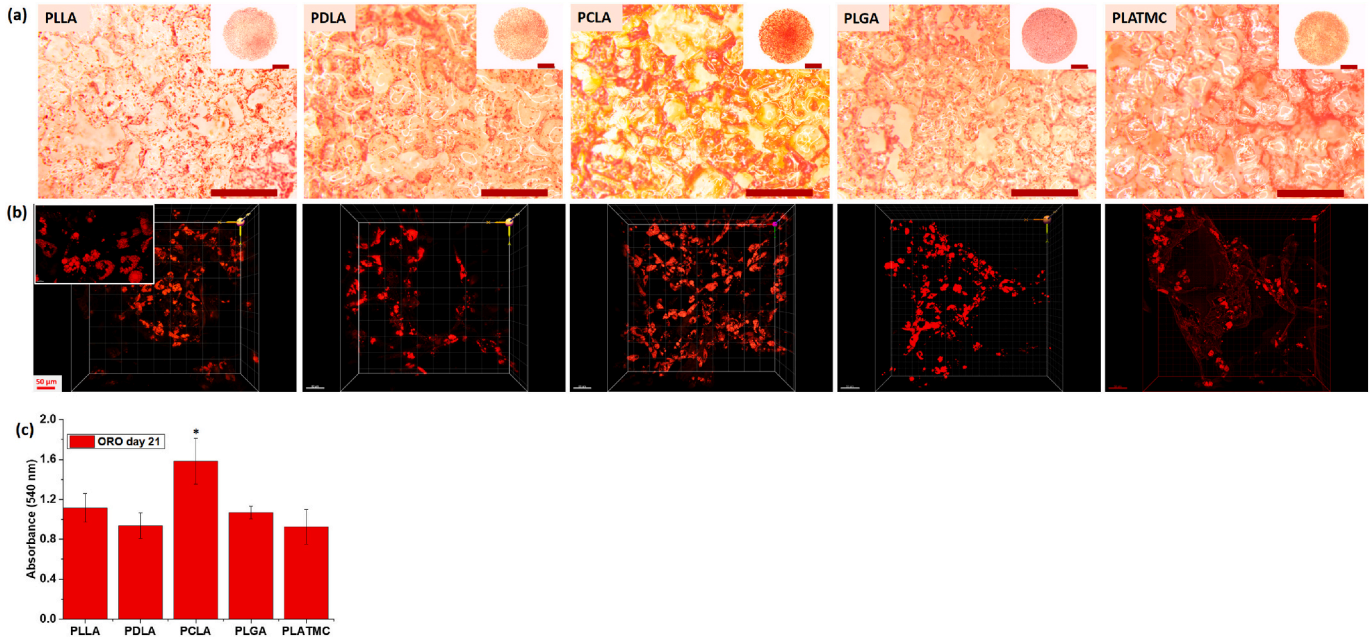

Fig. 8. ORO and AdipoRed™ staining of ASC at day 21 cultured in AM. (a) Stereomicrograph of the stained lipid droplets stained using ORO dye (red) (Scale bar = 500 μm). Inset shows, picture of complete scaffolds (scale bar = 2 mm) (b) 3D confocal micrograph of the stained lipid droplets showing the distribution on and inside the scaffolds (scale bar = 50 μm). Insets shows, the zoomed image of lipid droplets (scale bar 10 μm). (c) Quantification of ORO staining of the lipid droplets. * shows a significant difference ($P < 0.05$). (For interpretation of the references to color in this figure legend, the reader is referred to the web version of this article.)

differentiation process and it is also regulating the lipid droplets formation in the mature adipocytes [60,61]. We found that PLLA showed significantly less expression of LPL than others while PDLA, PCLA, PLGA, and PLATMC had no significant difference between each other. ADIPOQ is a gene encodes for adipokine, a protein hormone secreted by the mature adipocytes that enhances the differentiation process further and increases lipid droplets formation [62]. We assessed the expression of ADIPOQ, and the result showed that PCLA had a significantly higher expression of ADIPOQ than PLLA and other scaffolds did not show any significant difference.

ASC in the presence of adipogenic supplements becomes mature adipocytes and accumulates the lipid droplets which is considered as one of the signs of adipogenic differentiation. We used ORO dye to stain and quantify the formed lipid droplets. Additionally, AdipoRed™ dye was used to stain the intracellular lipid droplets, visualized using a confocal laser microscope.

Result summarized in Fig. 8 showed that PCLA scaffolds had significantly higher amount of lipid droplets than others, while there was no significant difference observed in lipid droplet accumulation in cells cultured on PLLA, PDLA, PLGA, and PLATMC. This indicates enhanced adipogenesis in cells cultured on PCLA scaffolds. It has been shown previously that rigid surfaces enhanced osteogenic differentiation of the stem cells, whereas soft substrates favored adipogenic differentiation [54]. Adipose tissue is comprised of liquid and solid substances and behaves like a viscoelastic material naturally. Moreover, in adipose tissue, during adipogenesis, the elastic component increases due to deposition of collagen matrix and adipocytes stiffness changes due to cytoskeleton reorganization to contain the large lipid droplets [63]. Hence a material having a good elastic response might enhance adipogenesis. PCLA exhibited higher pliability compared to PLLA, PDLA, and PLGA due to the incorporation of CL in the chains. This could be the reason for enhanced lipid droplet formation on PCLA scaffolds. Interestingly, PLATMC also exhibited pliability due to the presence of TMC but lipid droplet formation was not enhanced compared to PLLA, PDLA, and PLGA. The substrate stiffness sensitivity of a stem cell is more like a bell-shaped distribution across the physiological stiffness range [64]. Therefore, it can be speculated that a certain degree of crystallinity (a X_c of 20% for PCLA scaffolds against the amorphous PLATMC scaffolds), influences the local stiffness which MSC sense and may be helping in rearranging the cytoskeleton accordingly. Thus, a better structural support essentially enhances the lipid droplets formation. Hence, in the future, a detailed investigation is needed to understand the effect of local stiffness and signaling pathways on MSC differentiation using PCLA and PLATMC scaffolds along with *in vivo* exploration of adipogenic differentiation.

Taken together, adipogenic differentiation results suggest that PCLA is the most suitable polymer, followed by PLATMC, for adipose tissue regeneration. In addition, we have shown that PCLA and PLATMC are suitable to be used in additive manufacturing technique allowing customized pliable scaffolds with high precision which is not possible with conventional salt-leaching technique and these can be used in different type of 3D printers as well to create 3D scaffolds with high fidelity [43,65,66].

3.3. Characterization of scaffold properties after EB and ETO sterilization

Sterilization of the biomaterials or of any medical devices used for *in vivo* applications is a critical step. Thus, an effective technique is required which does not cause any physical and chemical alteration that can further compromise their functional characteristics and structural integrity. Our results from the biological study above suggested that mechanical properties of the scaffolds were crucial in stem cell proliferation and adipogenic differentiation. Consequently, we wanted to understand how different sterilization methods influence the scaffold properties. We, therefore, performed sterilization using EB and ETO, which are the most common techniques for medical devices, and determined if the sterilization methods influenced the polymer properties.

For EB sterilization, we used a dose of 25 kGy to sterilize the scaffolds. This is a minimum dose routinely used to sterilize the medical devices, biological tissue, and pharmaceutical products as per the International Organization for Standardization (ISO) [67]. Additionally, this dose can provide a sterility assurance (SAL) level of 10^{-6}.

EB radiation is generated by an accelerating stream of electrons where the dose of the radiation depends on the emitting source. Upon EB exposure, the formation of reactive oxygen species occurs (ROS) by the transfer of energy to the valence electron. The generation of ROS species further damages the cellular components of the microorganism. Moreover, EB directly causes the breakage of DNA/RNA of the microorganisms that causes the death of the microorganisms [68]. This is the same process that occurs when gamma radiation is used for sterilization, both radiation sterilization technique eliminates bacteria (gram-negative and positive), fungi, virus, and some bacterial spores [69].

Each sterilization process comes with its own pros and cons. Despite being an effective method of sterilization for 3D scaffolds used in tissue engineering applications, radiation sterilization is known to cause an alternation in the polymer properties and chemical structure. The generated free radicals can react with the polymer and thus create branches, crosslinking, or shorten the polymeric chains by chain-scission or unzipping reactions [70,71]. However, the extent of unwanted reaction depends on many factors such as polymer macroscopic structure, the structure of the monomeric units constituting the macromolecules, the dose rate, the dose itself, and the sterilization environment wherein material had been placed. We, therefore, characterized the thermal, chemical, and mechanical properties of the scaffolds, and M_n of the polymers after sterilization (AS) and compared to that of before sterilization (BS).

The molar mass of the polymer is influenced by the degradation generated by the free radicals during EB. SEC was used to determine the changes in the M_n and the data before and after sterilization is compared in Table 3 and Fig. 9a. All polymers had a significant decrease in the M_n and increase in Đ which agrees with previous reports. These results indicate that the possible degradation mechanism could be chain scission [72]. The excited electronic states formed to release the extra energy which causes the formation of radicals responsible for chain scission in both the amorphous and crystalline regions. It has also been shown that a high dose of EB triggers other chemical reactions such as crosslinking [73,74]. Although cross-linking results increase in the M_n of the polymer, we did not see any increase in M_n assuming no such reactions occurred for the polymers.

Among all the polymers, PDLA showed the highest decrease in M_n due to the amorphous nature of the polymer, which makes it more prone to being affected due to losing packing. PLLA, which is a semi-crystalline material (X_c = 51%), showed comparatively less degradation because the crystalline region has compact packing of the polymer chains which makes it less vulnerable to degradation [37,75]. PLGA was also semi-crystalline but crystalline content was much lower (3.5%) compare to that of PLLA, and it showed a 47% reduction in the M_n. Loo et al. previously showed that upon EB exposure, PLLA and PLGA were more susceptible to chain scission than crosslinking and the ratio of crosslinking to chain scission was higher for PLGA than PLLA. This indicate that PLGA is more susceptible than PLLA toward EB exposure due to less crystallinity and stable radical formation because in the crystalline phase free radicals can recombine hence reducing the chain-scission [70]. Structure of the constitutional units in a copolymer and their susceptibility to form a radical species affect the extent of the degradation. Interestingly, PCLA showed the lowest reduction (21%) among all polymers. Previously, researchers have shown that the incorporation of the caprolactone into PLA increased the stability of the copolymer toward EB [37,76]. Despite having an amorphous nature of PLATMC, it showed the lowest reduction (32%) after the PCLA. Previously, it has been shown that a longer block of trimethylene carbonate (TMC) in a

Table 3
Characterization of the scaffold's thermal properties and molar mass of the polymer. BS (before sterilization) and AS (after sterilization).

Polymer name		M_n (kg mol^{-1})[a]	Đ[a]	T_g (°C)[b]	T_m (°C)[b]	T_c (°C)[b]	X_c (%)[c]	Compressive moduli[d] (kPa)
PLLA	BS	196 ± 10	1.3	60	180	–	51	818 ± 216
	AS	120 ± 2	1.5	60	180	–	49	715 ± 136
PDLA	BS	178 ± 6	1.4	59	–	–	–	595 ± 158
	AS	88 ± 6	1.5	59	–	–	–	582 ± 210
PCLA	BS	138 ± 1	1.5	27	160	–	20	80 ± 10
	AS	109 ± 4	1.6	27	160	–	18	71 ± 14
PLGA	BS	249 ± 6	1.3	60	153	–	3.5	736 ± 99
	AS	134 ± 6	1.4	61	158	102	15	691 ± 138
PLATMC	BS	154 ± 3	1.4	28	–	–	–	261 ± 92
	AS	104 ± 1	1.5	38	149	–	1.4	246 ± 90

[a] Number average molar mass and dispersity determined by SEC using calibration curve from polystyrene standard with low dispersity in $CHCl_3$.
[b] T_g, T_m, T_c and X_c data were obtained from the first run of DSC.
[c] The crystallinity, X_c, (%) was calculated from the first heating run.
[d] The compressive moduli were determined using a compression test at RT in dry conditions, before and after EB sterilization.

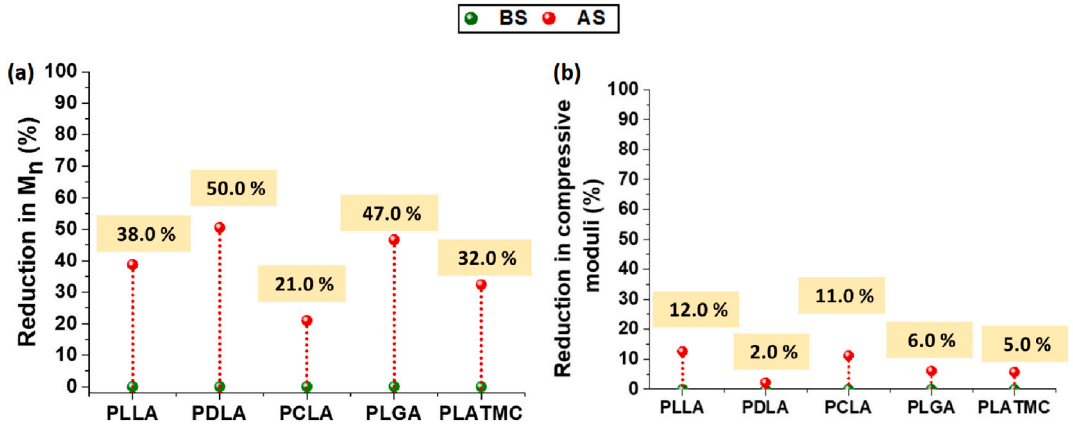

Fig. 9. 3D scaffolds were sterilized using EB and scaffold properties were compared before and after sterilization at RT. (a) Change in the M_n of the polymer (b) Change in compressive moduli before and after sterilization.

random copolymer of lactide and TMC reduced radical formation and had a faster radical decay when compared to lactide rich compositions [77]. Additionally, lactide units give rise to alkoxyl and acetyl radical upon chain-session of ester linkage while the TMC segment produces alkyl radicals that undergo fast decay [77].

Results from thermal properties before and after sterilization are compared in Table 3. It was seen that PLLA, PDLA, and PCLA thermal properties were not significantly affected by the EB. However, a decreasing trend in crystallinity (X_c) of PLLA and PCLA was seen, possibly due to the chain scission of the polymer chains. We observed signals in the ^{13}C NMR (data not reported) spectra indicating that transesterification reaction could have occurred. PDLA was completely amorphous both before and after sterilization. The thermal properties of the PLGA and PLATMC were affected more by the EB. We observed an increasing trend in physical properties. For PLGA, before sterilization T_m and X_c were 153 °C and 3.5%, correspondingly. Then, after EB sterilization, an increase in T_m and X_c observed which were 158 °C and 15%, respectively. In addition, a cold crystallization (T_c) peak was observed for the PLGA which was not seen in other scaffolds. It showed previously that the amorphous region in a copolymer is more affected upon the EB exposure wherein chain scission occurs, causing formation of short polymer chains. Indeed, PDLA and PLGA showed a 50% and 47% decrease in M_n, respectively (Fig. 9a). Eventually, these short chains have better mobility, can align themselves in close packing and give rise to form a crystalline region causing a T_c peak during the first heating run. It has been shown that after EB exposure PLGA can have branched or linear chains due to the recombination of free radicals. These linear chains allow dense packing compare to branched chain, results in a T_c peak [70].

PLATMC scaffolds showed a change in thermal properties after sterilization. We detected a significant increase in T_g from 28 to 38 °C but the T_c peak was not present. However, a melting peak was noticed which was not present before but X_c was negligible (1.3%). This can be attributed to the rearrangement of the short polymer chains into closer packing after EB exposure which makes it more stable and required higher energy for chain mobility and melts. In a recent study, it was shown that, when TMC content is higher (81%) in a copolymer with lactide, a cross-linking reaction occurs after EB sterilization [77]. In addition, as cross-linking reactions occur, T_g increases and cross-linking also contributes to an increase in M_n. Interestingly, we did not find an increase in M_n, therefore, this rise in T_g could be due to the rearrangement of the polymer chains only after exposure to EB.

It is also known that a reduction in the M_n leads to a decrease in the mechanical properties of the scaffolds. This affects further scaffolds degradation and cell-material interactions. We compared the compressive modulus of the scaffolds before and after sterilization. Fig. 9b shows the change in moduli before and after sterilization. A trend toward a decrease was observed among all scaffolds, but it was not statistically significant. This could be due to the fact that M_n of a polymer affects mechanical properties up to a certain limit, after which it is independent of the M_n [78].

We further performed ETO sterilization of the scaffolds, processed at room temperature, and evaluated the physical and chemical characteristics of the scaffolds. The results showed neither change in thermal properties nor in M_n, the values were similar to the polymers in the unsterilized scaffolds (Table 3). Therefore, we did not evaluate further the mechanical properties of the scaffolds. Analogous findings have been reported for a balloon implant, made of a similar PCLA, which after

three ETO sterilization cycles did not show any change in the polymer properties [79]. Similarly, the sterilization method did not have any effect on mechanical strength or on the *in vitro* hydrolysis rate [80].

Based on these results, it can be concluded that ETO sterilization would be a more suitable sterilization method for degradable polymers than EB. EB led to changes in polymer properties which would affect the interaction between ASC and the scaffolds and further influence the clinical *in vivo* performance of the implant/device.

4. Conclusions

A systematic evaluation of lactide based copolymers scaffolds allowed the understanding of how the physical, chemical, and mechanical properties of the materials influence stem cell adipogenesis. This information can be used to select an appropriate polymer to fabricate a resorbable medical implant/device for adipose/soft tissue engineering. The result showed that T_g and crystallinity affected mechanical properties in a synergistic manner. In contrast to PLLA, PDLA, and PLGA, the T_g of PCLA and PLATMC was below 37 °C, therefore scaffolds made of these polymers were more pliable and softer.

In vitro cell-material interactions revealed that all the scaffolds supported attachment, proliferation and differentiation of ASC. However, attachment and proliferation were enhanced for PCLA and PLATMC scaffolds as a consequence of their mechanical properties, being similar to those of adipose tissue. Moreover, PCLA scaffolds showed also an increased adipogenic differentiation. Therefore, it is concluded that PCLA should be the first choice, and secondly, PLATMC, among the polymers examined, for developing clinical implants. Finally, sterilization of the scaffolds by electron beam and ethylene oxide was performed. The results suggested that medical devices or implants from aforementioned polymers should be sterilized using ethylene oxide since it does not change native polymer properties. Further, extra attention must be given to material properties when using electron beam sterilization, since this led to a decrease in molar mass, a rise in crystallinity and change in mechanical properties, where PCLA was the least affected.

Our findings, therefore, contribute to increase competence around how degradable polymers influence the cells and also to give precise direction to select the most suitable polymer for the adipose/soft tissue application. Future research should include *in vivo* exploration of these polymeric scaffold's degradation and assessment of adipogenic differentiation.

Ethical approval

Ethical approval was obtained Regional committees for medical and Health Research Ethics (2013/1248/REK). Human fat tissue samples were obtained from patients who underwent routine surgery at Haukeland University Hospital, Bergen, Norway, with proper consent.

Author statement

Shubham Jain: Conceptualization, Methodology, Investigation, Formal analysis, Writing - Original Draft.

Mohammed Ahmad Yassin: Conceptualization, Methodology, Supervision, Writing - Review & Editing.

Tiziana Fuoco: Conceptualization, Methodology, Formal analysis, Supervision, Writing - Review & Editing.

Samih Mohamed-Ahmed: Resources, Writing - Review & Editing.

Hallvard Vindenes: Resources.

Kamal Mustafa: Resources, Review, Funding acquisition.

Anna Finne-Wistrand: Conceptualization, Methodology, Resources, Supervision, Writing - Review & Editing, Project administration, Funding acquisition.

Declaration of competing interest

The authors declare that they have no known competing financial interests or personal relationships that could have appeared to influence the work reported in this paper.

Acknowledgements

The researchers would like to thank Swedish Foundation for Strategic Research (SSF; RMA15-0010) for providing necessary support for this work. TROND MOHN Foundation, Norway (BFS2018TMT10) and Research Council of Norway (project no. 273551) for providing necessary financial support for this research. The molecular imaging center (MIC) of the University of Bergen is acknowledged for access to confocal microscopy.

References

[1] A. Casadei, R. Epis, L. Ferroni, I. Tocco, C. Gardin, E. Bressan, S. Sivolella, V. Vindigni, P. Pinton, G. Mucci, Biomed. Res. Int. 2012 (2012) 1–12.
[2] S.R. Coleman, J.H. Carraway, Plast. Reconstr. Surg. 110 (2002) 1731–1744.
[3] I. Nakajima, H. Aso, T. Yamaguchi, K. Ozutsumi, Differentiation 63 (1998) 193–200.
[4] S.-W. Cho, S.-S. Kim, J.W. Rhie, H.M. Cho, C.Y. Choi, B.-S. Kim, Biomaterials 26 (2005) 3577–3585.
[5] E. Yuksel, J. Choo, M. Wettergreen, M. Liebschner, Seminars in Plastic Surgery, Thieme Medical Publishers, 2005, p. 261.
[6] J.H. Choi, J.M. Gimble, K. Lee, K.G. Marra, J.P. Rubin, J.J. Yoo, G. Vunjak-Novakovic, D.L. Kaplan, Tissue Eng. B Rev. 16 (2010) 413–426.
[7] Y. Sun, A. Finne-Wistrand, A.C. Albertsson, Z. Xing, K. Mustafa, W.J. Hendrikson, D.W. Grijpma, L. Moroni, J. Biomed. Mater. Res., Part A 100 (2012) 2739–2749.
[8] D. Pappalardo, T.R. Mathisen, A. Finne-Wistrand, Biomacromolecules 20 (2019) 1465–1477.
[9] R.P. Pawar, S.U. Tekale, S.U. Shisodia, J.T. Totre, A.J. Domb, Recent Pat. Regener. Med. 4 (2014) 40–51.
[10] P. Feng, S. Peng, C. Shuai, C. Gao, W. Yang, S. Bin, A. Min, ACS Appl. Mater. Interfaces 12 (2020) 46743–46755.
[11] C. Bartus, C. William Hanke, E. Daro-Kaftan, Dermatol. Surg. 39 (2013) 698–705.
[12] B.L. Eppley, M. Reilly, J. Craniofac. Surg. 8 (1997) 116–120.
[13] P. Mäkelä, T. Pohjonen, P. Törmälä, T. Waris, N. Ashammakhi, Biomaterials 23 (2002) 2587–2592.
[14] C. Patrick Jr., B. Zheng, C. Johnston, G.P. Reece, Tissue Eng. 8 (2002) 283–293.
[15] R.A. Jain, Biomaterials 21 (2000) 2475–2490.
[16] M.P. Chhaya, E.R. Balmayor, D.W. Hutmacher, J.-T. Schantz, Sci. Rep. 6 (2016) 28030.
[17] M.P. Chhaya, F.P.W. Melchels, B.M. Holzapfel, J.G. Baldwin, D.W. Hutmacher, Biomaterials 52 (2015) 551–560.
[18] A.P. Pêgo, A.A. Poot, D.W. Grijpma, J. Feijen, J. Control. Release 87 (2003) 69–79.
[19] W.-J. Li, J.A. Cooper Jr., R.L. Mauck, R.S. Tuan, Acta Biomater. 2 (2006) 377–385.
[20] S. Ribeiro, A.M. Carvalho, E.M. Fernandes, M.E. Gomes, R.L. Reis, Y. Bayon, D. I. Zeugolis, Acta Biomater. 121 (2020) 302–315.
[21] S. Behtaj, F. Karamali, E. Masaeli, Y.G. Anissimov, M. Rybachuk, Biochem. Eng. J. 166 (2020), 107846.
[22] S.J. Hollister, Nat. Mater. 4 (2005) 518–524.
[23] T. Fuoco, A. Ahlinder, S. Jain, K. Mustafa, A. Finne-Wistrand, Biomacromolecules 21 (2019) 188–198.
[24] M.A. Yassin, T. Fuoco, S. Mohamed-Ahmed, K. Mustafa, A. Finne-Wistrand, Macromol. Biosci. 19 (2019), 1900049.
[25] M. Zhu, W. Li, X. Dong, X. Yuan, A.C. Midgley, H. Chang, Y. Wang, H. Wang, K. Wang, P.X. Ma, Nat. Commun. 10 (2019) 1–14.
[26] B. Chan, K. Leong, Eur. Spine J. 17 (2008) 467–479.
[27] D.A. Young, Y.S. Choi, A.J. Engler, K.L. Christman, Biomaterials 34 (2013) 8581–8588.
[28] N. Saxena, P. Mogha, S. Dash, A. Majumder, S. Jadhav, S. Sen, J. Cell Sci. 131 (2018).
[29] S. Jain, T. Fuoco, M.A. Yassin, K. Mustafa, A. Finne-Wistrand, Biomacromolecules 21 (2019) 388–396.
[30] C. Shuai, L. Yu, P. Feng, Y. Zhong, Z. Zhao, Z. Chen, W. Yang, Mater. Chem. Front. 4 (2020) 2398–2408.
[31] S. Jain, S.R.K. Meka, K. Chatterjee, ACS Biomater. Sci. Eng. 2 (2016) 1376–1385.
[32] H. Liu, A. Ahlinder, M.A. Yassin, A. Finne-Wistrand, T.C. Gasser, Mater. Des. 188 (2020), 108488.
[33] N.P. Tipnis, D.J. Burgess, Int. J. Pharm. 544 (2018) 455–460.
[34] Z. Dai, J. Ronholm, Y. Tian, B. Sethi, X. Cao, J. Tissue Eng. 7 (2016), 2041731416648810.
[35] M. Savaris, V. Dos Santos, R. Brandalise, Mater. Sci. Eng. C 69 (2016) 661–667.
[36] G.C. Mendes, T.R. Brandao, C.L. Silva, Am. J. Infect. Control 35 (2007) 574–581.
[37] K. Odelius, P. Plikk, A.-C. Albertsson, Biomaterials 29 (2008) 129–140.
[38] P. Rychter, N. Śmigiel-Gac, E. Pamuła, A. Smola-Dmochowska, H. Janeczek, W. Prochwicz, P. Dobrzyński, Materials 9 (2016) 64.
[39] K. Odelius, P. Plikk, A.-C. Albertsson, Biomacromolecules 6 (2005) 2718–2725.

[40] E. Fischer, H.J. Sterzel, G. Wegner, Colloid Polym. Sci. 251 (1973) 980–990.
[41] S. Mohamed-Ahmed, I. Fristad, S.A. Lie, S. Suliman, K. Mustafa, H. Vindenes, S. B. Idris, Stem Cell Res. Ther. 9 (2018) 168.
[42] S. Jain, S.R.K. Meka, K. Chatterjee, Biomed. Mater. 11 (2016), 055007.
[43] S. Jain, M.A. Yassin, T. Fuoco, H. Liu, S. Mohamed-Ahmed, K. Mustafa, A. Finne-Wistrand, J. Tissue Eng. 11 (2020), 2041731420954316.
[44] Q. Hou, D.W. Grijpma, J. Feijen, Biomaterials 24 (2003) 1937–1947.
[45] F. Guilak, D.M. Cohen, B.T. Estes, J.M. Gimble, W. Liedtke, C.S. Chen, Cell Stem Cell 5 (2009) 17–26.
[46] M. Bartnikowski, T.J. Klein, F.P. Melchels, M.A. Woodruff, Biotechnol. Bioeng. 111 (2014) 1440–1451.
[47] P. Tan, S. Teoh, Mater. Sci. Eng. C 27 (2007) 304–308.
[48] J. Broström, A. Boss, I.S. Chronakis, Biomacromolecules 5 (2004) 1124–1134.
[49] E.H. Immergut, H.F. Mark, Adv. Chem. Ser. 48 (1965) 1–26.
[50] A.I. Caplan, J. Cell. Physiol. 213 (2007) 341–347.
[51] M. Fan, Y. Ma, Z. Zhang, J. Mao, H. Tan, X. Hu, Mater. Sci. Eng. C 56 (2015) 311–317.
[52] A.J. Katz, A. Tholpady, S.S. Tholpady, H. Shang, R.C. Ogle, Stem Cells 23 (2005) 412–423.
[53] A.J. Engler, S. Sen, H.L. Sweeney, D.E. Discher, Cell 126 (2006) 677–689.
[54] T. Zhang, S. Lin, X. Shao, S. Shi, Q. Zhang, C. Xue, Y. Lin, B. Zhu, X. Cai, J. Cell. Physiol. 233 (2018) 3418–3428.
[55] W. Zhao, X. Li, X. Liu, N. Zhang, X. Wen, Mater. Sci. Eng. C 40 (2014) 316–323.
[56] M. Vatankhah-Varnosfaderani, W.F. Daniel, M.H. Everhart, A.A. Pandya, H. Liang, K. Matyjaszewski, A.V. Dobrynin, S.S. Sheiko, Nature 549 (2017) 497–501.
[57] A. Vahdati, D.R. Wagner, J. Biomech. 46 (2013) 1554–1560.
[58] A. Gefen, B. Dilmoney, Technol. Health Care 15 (2007) 259–271.
[59] S.R. Farmer, Cell Metab. 4 (2006) 263–273.
[60] D. Moseti, A. Regassa, W.-K. Kim, Int. J. Mol. Sci. 17 (2016) 124.
[61] T.C. Walther, R.V. Farese Jr., Annu. Rev. Biochem. 81 (2012) 687–714.
[62] Y. Fu, N. Luo, R.L. Klein, W.T. Garvey, J. Lipid Res. 46 (2005) 1369–1379.
[63] M.K. DeBari, R.D. Abbott, Int. J. Mol. Sci. 21 (2020) 6030.
[64] G. De Santis, A.B. Lennon, F. Boschetti, B. Verhegghe, P. Verdonck, P. J. Prendergast, Eur. Cells Mater. 22 (2011) 202–213.
[65] A. Ahlinder, S. Charlon, T. Fuoco, J. Soulestin, A. Finne-Wistrand, Polym. Degrad. Stab. 181 (2020), 109372.
[66] A. Ahlinder, T. Fuoco, Á. Morales-López, M.A. Yassin, K. Mustafa, A. Finne-Wistrand, J. Appl. Polym. Sci. 137 (2020) 48550.
[67] G. Mendes, T.R. Brandão, C.L. Silva, Ethylene Oxide (EO) Sterilization of Healthcare Products, Sterilisation of Biomaterials and Medical Devices, Elsevier, 2012, pp. 71–96.
[68] M.M. Cox, J.R. Battista, Nat. Rev. Microbiol 3 (2005) 882–892.
[69] M.H.F. Spoto, C.R. Gallo, A.R. Alcarde, M.S.D.A. Gurgel, L. Blumer, J.M.M. Walder, R.E. Domarco, Sci. Agric. 57 (2000) 389–394.
[70] J. Loo, C. Ooi, F. Boey, Biomaterials 26 (2005) 1359–1367.
[71] M. El Fray, A. Bartkowiak, P. Prowans, J. Slonecki, J. Mater. Sci. Mater. Med. 11 (2000) 757–762.
[72] G. Scott, Mechanisms of Polymer Degradation and Stabilisation, Springer, 1990.
[73] L. Montanari, F. Cilurzo, L. Valvo, A. Faucitano, A. Buttafava, A. Groppo, I. Genta, B. Conti, J. Control. Release 75 (2001) 317–330.
[74] T. Kelen, Polymer Degradation, VNR, New York, 1983.
[75] S.C.J. Loo, C.P. Ooi, Y.C.F. Boey, Polym. Degrad. Stab. 83 (2004) 259–265.
[76] M. Walo, G. Przybytniak, A. Nowicki, W. Świeszkowski, J. Appl. Polym. Sci. 122 (2011) 375–383.
[77] A. Adamus-Wlodarczyk, R.A. Wach, P. Ulanski, J.M. Rosiak, M. Socka, Z. Tsinas, M. Al-Sheikhly, Polymers 10 (2018) 672.
[78] R.W. Nunes, J.R. Martin, J.F. Johnson, Polym. Eng. Sci. 22 (1982) 205–228.
[79] M. Haim Zada, A. Kumar, O. Elmalak, G. Mechrez, A.J. Domb, ACS Omega 4 (2019) 21319–21326.
[80] W.S. Pietrzak, J. Craniofac. Surg. 21 (2010) 177–181.
[81] S.C. Baker, G. Rohman, J. Southgate, N.R. Cameron, Biomaterials 30 (2009) 1321–1328.